Biochemical Engineering Journal 55 (2011) 108–118

Contents lists available at ScienceDirect

Biochemical Engineering Journal

journal homepage: www.elsevier.com/locate/bej

Improving the prediction of *Pseudomonas putida* mt-2 growth kinetics with the use of a gene expression regulation model of the TOL plasmid

Michalis Koutinas[a], Alexandros Kiparissides[a], Ming-Chi Lam[a,b], Rafael Silva-Rocha[c], Miguel Godinho[b], Victor de Lorenzo[c], Vitor A.P. Martins dos Santos[b,d], Efstratios N. Pistikopoulos[a], Athanasios Mantalaris[a,*]

[a] *Biological Systems Engineering Laboratory, Centre for Process Systems Engineering, Department of Chemical Engineering and Chemical Technology, South Kensington Campus, Imperial College London, SW7 2AZ London, United Kingdom*
[b] *Systems and Synthetic Biology Group, Helmholtz Center for Infection Research (HZI), Inhoffenstrasse 7, D-38124 Braunschweig, Germany*
[c] *Centro Nacional de Biotecnologia, Consejo Superior de Investigaciones Cientificas, Darwin 3, Cantoblanco, 28049 Madrid, Spain*
[d] *Chair for Systems and Synthetic Biology, Wageningen University, Dreijenplein 310, 6703 HB Wageningen, The Netherlands*

ARTICLE INFO

Article history:
Received 15 September 2010
Received in revised form 21 March 2011
Accepted 27 March 2011
Available online 2 April 2011

Keywords:
Dynamic modelling
pWW0 (TOL) plasmid
Genetic circuit
Pseudomonas putida
m-Xylene

ABSTRACT

The molecular and genetic events responsible for the growth kinetics of a microorganism can be extensively influenced by the presence of mixtures of substrates leading to unusual growth patterns, which cannot be accurately predicted by mathematical models developed using analogies to enzyme kinetics. Towards this end, we have combined a dynamic mathematical model of the *Ps*/*Pr* promoters of the TOL (pWW0) plasmid of *Pseudomonas putida* mt-2, involved in the metabolism of *m*-xylene, with the growth kinetics of the microorganism to predict the biodegradation of *m*-xylene and succinate in batch cultures. The substrate interactions observed in mixed-substrate experiments could not be accurately described by models without directly specifying the type of interaction even when accounting for enzymatic interactions. The structure of the genetic circuit–growth kinetic model was validated with batch cultures of mt-2 fed with *m*-xylene and succinate and its predictive capability was confirmed by successfully predicting independent sets of experimental data. Our combined genetic circuit–growth kinetic modelling approach exemplifies the critical importance of the molecular interactions of key genetic circuits in predicting unusual growth patterns. Such strategy is more suitable in describing bioprocess performance, which current models fail to predict.

1. Introduction

Microbial growth kinetics is an essential tool for the design of optimal bioprocesses. Despite more than half a century of research, many fundamental questions about the validity and application of growth kinetics are still unanswered [1]. One of the various cases in biotechnology where understanding of the kinetics of microbial growth is limited is when a culture is grown on mixed-substrates [2]. A multitude of utilisation patterns may occur depending on the metabolic effects of each compound [3] and various substrate interactions have been identified including sequential [4] and simultaneous [5] utilisation. Although substrate interactions can be either positively or negatively influenced by the presence of other compounds [6], in some cases unusual substrate interactions have been reported but not modelled [7].

In general there is no simple rule for the prediction of substrate interactions [8]. When no substrate interactions are identified, simple Monod terms [9] can be added in sum kinetics. However, if substrate interactions occur, growth rate equations accounting for these interactions are used [10]. Usually an analogy to enzyme kinetics is made, because if a reaction is enzyme catalysed then the inhibition of enzyme activity results in the inhibition of microbial growth by the same pattern. Nevertheless, although the determination of the model giving the most accurate description of the experimental data might suggest the mechanism of the interactions, this might not always hold true when unusual substrate interactions occur. Thus, for a certain combination of substrates none of the developed models may accurately fit the experimental data or the interaction indicated may not be valid for a wide range of conditions. Although the metabolic events taking place in mixed-substrate cultivation have been previously studied [6], the failure of models to predict the growth kinetics in some cases underlines the need for inclusion of the exact mechanism for the production of enzymes [11]. The genetic information required for the production of enzymes used for the metabolism of substrates in a certain

* Corresponding author. Tel.: +44 20 7594 5601; fax: +44 20 7594 5638.
E-mail address: a.mantalaris@imperial.ac.uk (A. Mantalaris).

1369-703X/$ – see front matter © 2011 Elsevier B.V. All rights reserved.
doi:10.1016/j.bej.2011.03.012

Nomenclature

$I_{1,2}$	interaction parameter of *m*-xylene on succinate [–]
$I_{2,1}$	interaction parameter of succinate on *m*-xylene [–]
i	inhibition constant [$mM^{-1}\ h^{-1}$]
$K_{I,1}$	*m*-xylene inhibition constant [mM]
$K_{I,1,2}$	*m*-xylene inhibition on succinate constant [mM]
$K_{I,1\text{-}P,2}$	*m*-xylene by-product inhibition on succinate constant [mM]
$K_{Iq,1,2}$	*m*-xylene inhibition on succinate consumption constant [mM]
$K_{Iq,1\text{-}P,2}$	*m*-xylene by-product inhibition on succinate consumption constant [mM]
$K_{Pr,XylR_i}$	$XylR_i$ translation coefficient [–]
$K_{S,1}$	*m*-xylene saturation constant [mM]
$K_{s,1}$	saturation constant for *m*-xylene consumption [mM]
$K_{S,2}$	succinate saturation constant [mM]
$K_{s,2}$	saturation constant for succinate consumption [mM]
$K_{SUC,Pr}$	inhibition constant of succinate on *Pr* promoter activity [mM^{-2}]
$K_{SUC,Ps}$	inhibition constant of succinate on *Ps* promoter activity [mM]
K_{XylR_a}	repression coefficient of *Pr* promoter (due to $XylR_a$ binding) [mM]
$K_{XylR_a,Ps}$	activation coefficient of *Ps* promoter [mM]
K_{XylR_i}	repression coefficient of *Pr* promoter (due to $XylR_i$ binding) [mM]
MWt_1	*m*-xylene molecular weight [mg $mmol^{-1}$]
n	exponent indicating the type of relation between μ_2 and S_2 [–]
$n_{Pr,a}$	hill coefficient of *Pr* promoter (due to $XylR_a$ binding) [–]
$n_{Pr,i}$	hill coefficient of *Pr* promoter (due to $XylR_i$ binding) [–]
$n_{Ps,a}$	hill coefficient of *Ps* promoter (due to $XylR_a$ binding) [–]
$q_{s,1}$	*m*-xylene metabolic quotient [$mM_{m\text{-xylene}}\ mg_{biomass}^{-1}\ h^{-1}$]
$q_{s,2}$	succinate metabolic quotient [$mM_{succinate}\ mg_{biomass}^{-1}\ h^{-1}$]
$r_{R,XylR}$	$XylR_a$ dissociation constant [$mM^{-1}\ h^{-1}$]
r_{XylR}	$XylR_i$ oligomerization constant [$mM^{-1}\ h^{-1}$]
$S_{0,1}$	initial *m*-xylene concentration [mM]
S_1	*m*-xylene concentration [mM]
S_2	succinate concentration [mM]
S_m	maximum *m*-xylene concentration above which growth is completely inhibited [mM]
S_θ	threshold *m*-xylene concentration below which there is no inhibition [mM]
t	time [h]
Y_1	yield coefficient for biomass on *m*-xylene [$mg_{biomass}\ mg_{m\text{-xylene}}^{-1}$]
Pr_{TC}	*Pr* promoter relative activity [–]
Ps_{TC}	*Ps* promoter relative activity [–]
$R_{max,1}$	maximum *m*-xylene metabolic quotient [$mmol_{m\text{-xylene}}\ mg_{biomass}^{-1}\ h^{-1}$]
$R_{max,2}$	maximum succinate metabolic quotient [$mmol_{succinate}\ mg_{biomass}^{-1}\ h^{-1}$]
X	biomass concentration [$mg\ L^{-1}$]
$XylR_a$	$XylR_a$ protein concentration [mM]
$XylR_i$	$XylR_i$ protein concentration [mM]

Greek letters

α_{Pr}	*Pr* promoter deactivation rate [h^{-1}]
α_{Ps}	*Ps* promoter deactivation rate [h^{-1}]
α_{XylR_i}	$XylR_i$ degradation/dilution rate [h^{-1}]
α_{XylR_a}	$XylR_a$ degradation/dilution rate [h^{-1}]
β_0	basal expression level of *Ps* promoter [h^{-1}]
β_{Pr}	maximal expression level of *Pr* promoter [h^{-1}]
β_{Ps}	maximal expression level of *Ps* promoter [h^{-1}]
β_{XylR_i}	maximal $XylR_i$ translation rate based on *Pr* activity [$mM\ h^{-1}$]
μ	specific growth rate of biomass [h^{-1}]
μ_1	specific growth rate of biomass on *m*-xylene [h^{-1}]
μ_2	specific growth rate of biomass on succinate [h^{-1}]
$\mu_{max,1}$	maximum specific growth rate of biomass on *m*-xylene [h^{-1}]
$\mu_{max,2}$	maximum specific growth rate of biomass on succinate [h^{-1}]

process, is encoded by genes existing in specific genetic circuits of the cells. Thus, the construction of mathematical models describing the molecular interactions regulating the transcription of these genes might provide the exact mechanism for substrate interactions.

Genetic circuits are groups of elements, which interact producing certain behaviour [12]. These elements include DNA binding regions for RNA polymerase starting transcription of DNA, DNA regions that terminate transcription, mRNA binding sequences for rRNA starting the translation of mRNA, proteins that regulate the synthesis and activity of other proteins, and motifs that determine mRNA and protein stability. Advanced genetic techniques may successfully identify the components of a circuit and the way these interact. With the application of these techniques, several naturally occurring genetic circuits have been studied recently, such as cell cycle regulatory systems [13], bistable switches [14], oscillating networks [15], and circadian clocks [16]. Therefore, given the fact that key genetic circuits are essential for survival and reproduction of microorganisms, the mechanisms of interactions between circuit components may well-define the distinct responses of various cellular functions to changes in the cells environment [17,18]. The current state of the art is rather limited to the work of Bettenbrock et al. [19] utilizing a dynamic gene regulation model of catabolite repression to describe the dynamic behaviour of various metabolites in *Escherichia coli*.

This study attempts to combine a mathematical model of a key genetic circuit with the growth kinetics of the host microorganism. To this end we have previously paved the way with the development of a mathematical model of the *Ps*/*Pr* node of the TOL plasmid encoded by *Pseudomonas putida* mt-2 [20]. Herein, we present a growth kinetic model of the strain and its coupling with the genetic circuit model, demonstrating a new approach for the improvement of growth kinetic models in cases where the use of quantitative genetic information is imperative. The parameter values of the combined model were estimated through independent experiments and its predictive capability was evaluated in a distinct experimental set-up. Analysis of the results showed that there is increased complexity in modelling substrates degradation and growth kinetics due to the substrate interactions. Although, the combined model offered an improved description of the process, different models, either accounting for interactions in analogy to enzyme kinetics or without directly specifying the type of interaction, were unsuccessful in describing the experiments. This modelling framework provides a solid basis for the development

of mechanistic mathematical models that consider key molecular interactions to predict unusual system performance that cannot be explained with currently existing models.

2. Materials and methods

2.1. Cell culture conditions

Subcultures of *P. putida* mt-2 were pregrown overnight at 30 °C in M9 minimal medium [21] supplemented with 15 mM succinate and an organic antifoaming agent (Antifoam 204, Sigma–Aldrich Company Ltd., UK). Triplicate cultures were prepared by diluting the overnight culture in minimal medium to an initial optical density of 0.1 at 600 nm. The minimal medium was supplemented with either succinate, *m*-xylene or a combination of the two substrates. The incubation of the cultures was performed using conical Erlenmeyer flasks with 2.35 L total volume (0.4 L culture volume), which were continuously stirred at 1250 rpm via a Heidolph MR 3001K (Heidolph, UK) magnetic stirrer. The flasks were filled with medium to one-fifth of their volume, to make sure that sufficient oxygen was available, and closed gas-tight with Teflon coated lids to avoid losses of the volatile organic compound. Biomedium and gas samples were collected from the flasks through a sampling port embedded on the lids and temperature was maintained constant at 30 °C in a constant temperature room facility. The same conditions were maintained at all times apart from the initial *m*-xylene and succinate concentrations, which varied for each experiment. Initial *m*-xylene and succinate concentrations for each experiment are given below. All chemicals used were obtained from Sigma–Aldrich Company Ltd. (UK) and were of ANALAR grade. *m*-Xylene was obtained from VWR International Ltd. (UK) 99% pure.

2.2. Experimental design

Three experiments were conducted to obtain the parameter values for the mathematical model, while its predictive capability was tested with an independent experiment. The initial concentrations for the two substrates were set at the following concentration levels for each experiment: (i) 0.9 mM *m*-xylene (*m*-xylene only experiment), (ii) 13.6 mM succinate (succinate only experiment), (iii) 1.04 mM *m*-xylene and 14 mM succinate (parameter estimation experiment), and (iv) 0.8 mM *m*-xylene and 14.1 mM succinate (predictive experiment). Biomass, *m*-xylene and succinate concentrations were monitored at certain time intervals using optical density, gas chromatography (GC) and high-pressure liquid chromatography (HPLC) analysis respectively, while real-time PCR was employed to determine gene expression. The above methods are described in detail in Sections 2.4 and 2.5.

2.3. Growth on the antifoaming agent

Intensive foaming formation was observed when the culture achieved dry cell weight concentration above 1 g L^{-1} in the presence of succinate. An antifoaming agent was used in all experiments, in order to avoid the formation of the foam. However, during the experiments, although a distinct lag-phase occurred where the substrate(s) were not consumed, an increase in biomass concentration was observed. In order to clarify that the increase in biomass concentration during that period was due to the addition of the antifoam, two flasks were inoculated in the presence or in the absence of the antifoaming agent. There was an increase in biomass concentration for the first 1.5 h following inoculation of the flask supplemented with antifoam, while biomass concentration started decreasing from the beginning of the flask that did not contain any antifoam indicating that the presence of the specific amount of antifoam added could support cellular growth for up to 1.5 h. The chemical composition of the antifoam was not defined and measurement of its concentration was not possible. Thus, for the first 1.5 h of each experiment the biomass produced due to the presence of the antifoam is given from best-fit time profile of its experimental values during the control experiment described above and it is neglected for the remaining of each experiment. The same concentration of antifoaming agent was used in all flasks.

2.4. Analyses

GC analysis was employed for determination of the *m*-xylene concentration in the gaseous and aqueous samples using an Agilent 6850 Series II Gas Chromatograph with an FID detector and a 'J&W Scientific' (Agilent Technologies UK Limited, UK) column with HP-1 stationary phase. Gaseous samples of 25 μL were injected into the GC and the temperature program run at 70 °C for 3 min and then increased to 80 °C at a rate of 5 °C min^{-1}. Biomedium *m*-xylene concentration was determined experimentally as previously described [20]. The coefficient of variation for 5 samples was 4.6% at a concentration level of 0.07 mM *m*-xylene. Succinate concentration was determined using HPLC on a Shimadzu liquid chromatograph LC-10AT (Shimadzu, UK) equipped with a SIL-10AD Shimadzu auto injector, a RID-10A Shimadzu refractive index detector and a CTO-10AC column oven. Samples were eluted with distilled water at a flow rate of 0.4 ml min^{-1} from an Aminex® HPX-87H (Bio-Rad Laboratories Ltd., UK) ion-exclusion organic acid analysis column at 55 °C. Biomedium samples were centrifuged and the supernatant was filtered through 0.2 μm filters to remove any remaining solids. 50 μl of the filtered sample was injected into the HPLC. The concentration of succinate was calculated interpolating from a previously established succinate calibration curve. The coefficient of variation for 3 samples was 0.1% at a concentration level of 4.38 mM succinate. Biomass concentration was determined by absorbance at 600 nm on a UV-2101PC scanning spectrophotometer (Shimadzu, UK) interpolating from a previously established dry weight calibration curve. The coefficient of variation for 5 samples was 4.2% at a concentration level of 583 $mg_{biomass}$ L^{-1}.

2.5. Isolation of total RNA, cDNA synthesis and quantitative real-time PCR

Quantitative real-time PCR (Q-PCR) was performed to determine the expression of *xylR*, *xylS* and *rpoN* genes during the experiments. 4.5 ml of biomedium samples were centrifuged for 4 min at 11,000 rpm. The supernatant solution was removed, while the cell pellet was quenched in liquid N_2 for 1 min and was stored at −80 °C. Total RNA was isolated from quenched cells using NucleoSpin® RNA II (Fisher Scientific Ltd., UK) and was eluted with 60 μl RNase-free water. Following the extraction, total RNA was used immediately for cDNA synthesis. cDNA was synthesised using iScript™ Select cDNA Synthesis Kit (Bio-Rad Laboratories Ltd., UK) using random priming and Q-PCR assays were performed on a Rotor-Gene 6000 (Qiagen Ltd., UK), using iQ™ SYBR® Green Supermix (Bio-Rad Laboratories Ltd., UK). For each reaction, 2 μl of cDNA (10 ng μl^{-1}) was mixed with 24 μl of the PCR solution. This solution contained 12.5 μl 1× iQ SYBR Green Supermix, 0.25 μl of forward primer (0.2 μM), 0.25 μl of reverse primer (0.2 μM) (Invitrogen Ltd., UK) and 11 μl of sterile water. PCR was carried out according to the following protocol: initial denaturation at 95 °C (3 min) followed by 50 cycles of 95 °C (20 s), 60 °C (30 s) and 72 °C (30 s), while a melting curve was generated for each reaction in order to ensure the specificity of each PCR product. Threshold cycle values (C_T) were calculated with the use of Rotor-Gene 6000 series software 1.7 (Qiagen Ltd., UK). Each Q-PCR was performed in duplicate. The coefficient of variation for 3 samples was 2.8% at a cDNA mass level of 10 ng_{cDNA} used for each reaction. The primer sequences and the

Table 1
Substrate inhibition models.

Publication	Authors	Equation
[24]	Andrews (1968)	$\mu_1 = \frac{\mu_{\max,1} S_1}{K_{S,1} + S_1 + (S_1^2/K_{I,1})}$ (1)
[25]	Aiba et al. (1968)	(2) $\mu_1 = \frac{\mu_{\max,1} S_1}{K_{S,1}+S_1} e^{(-S_1/K_{I,1})}$
[26]	Yano and Koga (1969)	$\mu_1 = \frac{\mu_{\max,1} S_1}{K_{S,1} + S_1 + (S_1^3/K_{I,1}^2)}$ (3)
[27]	Wayman and Tseng (1976)	(4) $\mu_1 = \frac{\mu_{\max,1} S_1}{K_{S,1}+S_1} - i(S_1 - S_\theta)$
[28]	Luong (1987)	(5) $\mu_1 = \frac{\mu_{\max,1} S_1}{K_{S,1}+S_1}\left(1 - \frac{S_1}{S_m}\right)^n$
[29]	Alagappan and Cowan (2001)	(6) $\mu_1 = \frac{\mu_{\max,1} S_1}{K_{S,1}+S_1+(S_1^2/K_{I,1})} - i(S_1 - S_\theta)$

method used for calculating the normalised levels of *xylR* and *xylS* mRNA expressions were performed as previously described [20].

2.6. Parameter estimation in gPROMS

All parameter estimation experiments and model simulations where carried out on an Intel® Core™2 Duo (E4600 – 2.4, 2.39) personal computer with 3.24 GB of RAM memory. Model simulations and parameter estimation experiments were implemented in the advanced process modelling environment gPROMS® [22], which is an equation-oriented modelling system used for building, validating and executing first-principles models within a flowsheeting framework. Parameter estimation in gPROMS is based on the Maximum Likelihood formulation, which provides simultaneous estimation of parameters in both the physical model of the process as well as the variance model of the measuring instruments. gPROMS attempts to determine values for the uncertain physical and variance model parameters, θ, that maximise the probability that the mathematical model will predict the measurement values obtained from the experiments. Assuming independent, normally distributed measurement errors, ε_{ijk}, with zero means and standard deviations, σ_{ijk}, this maximum likelihood goal can be captured through the following objective function Eq. (7):

$$\Phi = \frac{N}{2}\ln(2\pi) + \frac{1}{2}\min_\theta \left\{ \sum_{i=1}^{NE}\sum_{j=1}^{NVi}\sum_{k=1}^{NMij} \left[\ln(\sigma_{ihk}^2) + \frac{(\bar{z}_{ijk} - z_{ijk})^2}{\sigma_{ihk}^2} \right] \right\} \quad (7)$$

where N stands for total number of measurements taken during all the experiments, θ is the set of model parameters to be estimated, NE is the number of experiments performed, NV_i is the number of variables measured in the ith experiment and NM_{ij} is the number of measurements of the jth variable in the ith experiment. The variance of the kth measurement of variable j in experiment i is denoted as σ_{ijk}^2, while $\bar{z}_{ijk}$ is the kth measured value of variable j in experiment i and z_{ijk} is the kth (model-)predicted value of variable j in experiment i. The above formulation can be reduced to a recursive least squares parameter estimation if no variance model for the sensor is selected.

3. Results and discussion

3.1. Single-substrate biodegradation: m-xylene only

Subcultures of *P. putida* mt-2 were first grown in the presence of succinate and *m*-xylene as single substrates. The biodegradation of 0.9 mM *m*-xylene fed in a batch experiment was most accurately modelled assuming substrate inhibition, as noted by the experimental results presented in Fig. 1A, which is in agreement with previously developed models of *m*-xylene biodegradation by *P. putida* [23]. The Monod and various substrate inhibition models that have been used to describe the growth on *m*-xylene are provided in Eqs. (1)–(6) (Table 1). From the models propagated, although there were small differences between three of the models tested (Andrews, Yano and Koga, Wayman and Tseng), the Yano and Koga equation (3) showed the best fit (Supporting Fig. 1) and was selected to describe biomass growth on *m*-xylene. Furthermore, *m*-xylene consumption was modelled using Eq. (8), the specific *m*-xylene consumption rate was independently modelled using Eq. (9) and biomass concentration was expressed by Eq. (10).

Table 2
Parameter values used for model simulation.

Parameter	Value	95% Conf. interval	Units	Experiment
$I_{1,2}$	2.971	–	–	3
$I_{2,1}$	0	–	–	3
$K_{I,1}$	0.439	0.049	mM	1
$K_{I,1}$ [a]	0.465	0.044	mM	1
$K_{I,1,2}$	19.418	23	mM	3
$K_{I,\ 1\text{-}P,2}$	0.84	0.038	mM	3
$K_{Iq,1,2}$	7.248	2.3	mM	3
$K_{Iq,\ 1\text{-}P,2}$	0.823	0.028	mM	3
$K_{S,1}$	0.099	0.054	mM	1
$K_{S,1}$ [a]	0.096	0.04	mM	1
$K_{S,2}$	43.047	34	mM	2
$K_{s,2}$	45.781	–	mM	2
$R_{\max,1}$	0.076	6.9×10^{-4}	$\text{mmol}_{m\text{-xylene}}\ g_{\text{biom}}^{-1}\ h^{-1}$	1
$R_{\max,1}$ [a]	0.072	5.7×10^{-4}	$\text{mmol}_{m\text{-xylene}}\ g_{\text{biom}}^{-1}\ h^{-1}$	1
$R_{\max,2}$	0.029	4.4×10^{-4}	$\text{mmol}_{\text{succinate}}\ g_{\text{biom}}^{-1}\ h^{-1}$	2
$\mu_{\max,1}$	0.931	0.17	h^{-1}	1
$\mu_{\max,1}$ [a]	0.979	0.15	h^{-1}	1
$\mu_{\max,2}$	2.637	0.013	h^{-1}	2

1—Single-substrate biodegradation: *m*-xylene only; 2—single-substrate biodegradation: succinate only; 3—succinate–*m*-xylene mixture: parameter estimation experiment.

[a] Parameter value determined without information from the TOL model.

$$\frac{dS_1}{dt} = -\frac{1}{MWt_1}\frac{\mu_1}{Y_1}X \quad (8)$$

$$q_{s,1} = \frac{R_{\max,1} S_1}{K_{s,1} + S_1} = -\frac{1}{X}\frac{dS_1}{dt} \quad (9)$$

$$\frac{dX}{dt} = \mu_1 X \quad (10)$$

Combining Eqs. (8) and (9) the observed cell mass yield on *m*-xylene is given by Eq. (11).

$$Y_1 = \frac{1}{MWt_1}\frac{\mu_1}{R_{\max,1}}\left(1 + \frac{K_{s,1}}{S_1}\right) \quad (11)$$

If $S_1 \gg K_{s,1}$ and in the case where for a given initial substrate concentration the specific growth rate (μ_1) in the exponential growth phase is constant, then the observed cell mass yield is constant. Although this might not always hold true it is usually assumed that the yield coefficient is an average constant dependent on the initial substrate concentration ($S_{0,1}$), when the latter is much higher than the critical substrate concentration ($S_{0,1} \gg (K_{S,1}{K_{I,1}}^2)^{1/3}$) where μ_1 is maximum [30]. However, a constant yield cannot be present for a wide range of initial substrate concentrations when substrate inhibition is considered. Thus, for the experiments in the present study a new yield value was calculated for different initial *m*-xylene concentrations, using Eq. (12).

$$Y_1 = \frac{1}{MWt_1}\frac{\mu_{\max,1}}{R_{\max,1}}\frac{1}{1 + (K_{S,1}/S_{0,1}) + (S_{0,1}^2/K_{I,1}^2)} \quad (12)$$

The parameter values determined from the experiment presented in Fig. 1A are shown in Table 2. Monod-like models fail to

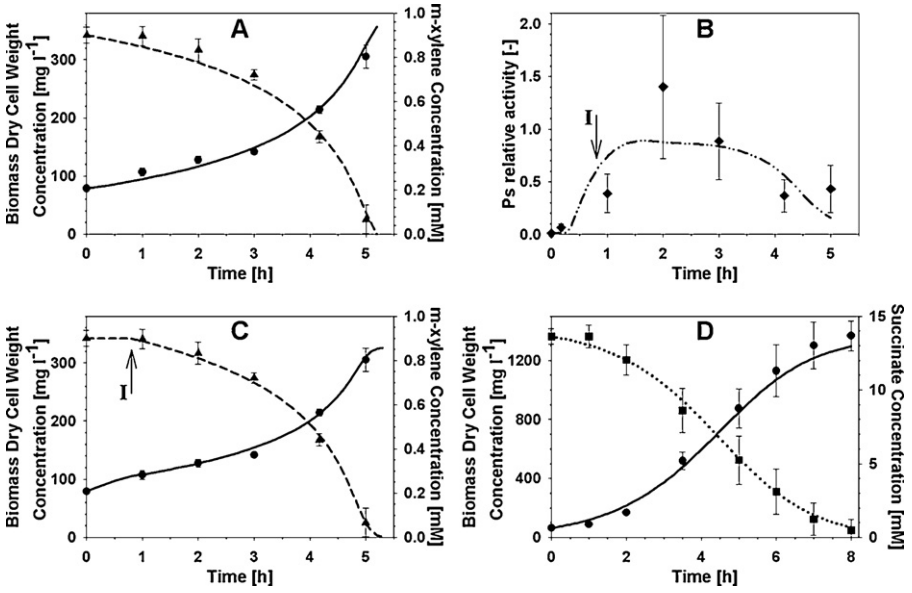

Fig. 1. Single-substrate batch biodegradation experiments. (A) *m*-Xylene biodegradation (predicted without genetic information), (B) *Ps* promoter relative activity, (C) *m*-xylene biodegradation (predicted by the combined model), and (D) succinate biodegradation. I: Beginning of *m*-xylene biodegradation; ●: biomass dry cell weight concentration – experimental; ■: succinate concentration – experimental; ▲: *m*-xylene concentration – experimental; ♦: *Ps* activity – experimental; ——: biomass dry cell weight concentration – predicted; . . . . . .: succinate concentration – predicted; – – –: *m*-xylene concentration – predicted; — · ·: *Ps* activity – predicted. The *Ps* promoter activity results are obtained as an average from 6 individual measurements for triplicate flasks at each time point and the error bars are calculated for standard deviation.

account for lag periods and consider the beginning of the exponential growth as their initial point [11]. Due to the fact that the model developed does not take into account the lag-phase, there was minor deviation of the model's prediction from the experimental results (Fig. 1A).

It is evident that a lag-phase occurred for the first 1 h following the introduction of *m*-xylene. One of the main reasons for true lag is the change in nutrition. Therefore, since the inoculum was pre-grown in succinate, the lag-phase might have been caused because the change in carbon source involves the induction of new enzymes catalysing the biodegradation of *m*-xylene. MT-2 is known to degrade *m*-xylene via the TOL pathway (Fig. 2), which is equipped with the enzymes for its oxidative catabolism [31]. The two gene operons of TOL (upper operon: *xyl*UWCMABN and *meta* operon: *xyl*XYZLTEGFJQKIH) encode the catabolic enzymes of the pathway, while two genes (*xylS* and *xylR*) control the regulation of transcription of the operons. These four transcriptional units are driven by four different promoters (upper operon: *Pu*, *meta* operon: *Pm*, *xyl*S gene: *Ps* and *xyl*R gene: *Pr*). Therefore, the time required to synthesise the optimum amount of the TOL enzymes can be directly (*Pu*) or indirectly (*Pm*) controlled by the master regulator of the system, the active form of XylR protein ($XylR_a$), which is activated by *m*-xylene [32]. For various known systems genes induced for biodegradation of new carbon sources constitute only a small fraction of the entire transcriptome reprogramming [33]. The transition from the lag to the accelerating growth phase is assumed to take place when *Ps*, which is activated by $XylR_a$, has its relative activity increased from its basal level by 65-fold, an amount which corresponds to the activation of the TOL pathway and consequently to the induction of its enzymes. A similar activation profile to that of *Ps* would be also expected for *Pu*, which is also activated by $XylR_a$.

The mathematical model of the *Ps*/*Pr* promoters of TOL previously developed [20], shown in Table 3, was used to calculate *Ps* promoter's activity over time (Fig. 1B). Thus, the duration of the lag-phase was estimated from the genetic circuit model and the growth kinetic model was used after the lag-phase to re-estimate the parameter values (Table 2). Therefore, by taking into account the duration of the lag-phase, the prediction of the combined model improved the description of the experiment (Fig. 1C), as confirmed by the high correlation coefficient values obtained between experimental and modelling results (Table 4). The development of the genetic circuit model is not further discussed in this paper, as this is readily available in the reference mentioned above.

3.2. Single-substrate biodegradation: succinate only

When high concentrations of an inhibitory substrate are fed in a bioprocess, an easily biodegradable substrate, such as succinate can

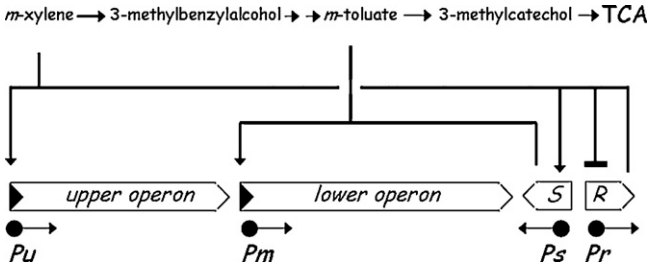

Fig. 2. Organization of the *m*-xylene biodegradation pathway born by the TOL plasmid pWW0. The figure sketches the reactions implicated in metabolism of this aromatic compound, including the stepwise oxidation of one methyl group of the substrate to an alcohol and eventually to a carboxylic acid, yielding *m*-toluate through the action of the enzymes encoded by the upper TOL pathway. *m*-Toluate is then deoxygenated to yield 3-methylcatechol, which is cleaved in *meta* and finally channelled into the Krebs cycle by means of the products of the lower or *meta* operon. The upper operon is transcribed from the σ^{54} promoter *Pu* upon activation by the cognate regulator of the pathway (XylR) bound to specific effectors. These include the substrate of the pathway (*m*-xylene) as well as the two first metabolic intermediates: 3-methylbenzylalcohol and 3-methylbenzylaldehyde. The lower operon is transcribed from the *Pm* promoter, which is activated by the *m*-toluate responsive activator XylS. *Pm* can be turned on either by XylS and *m*-toluate as a co-inducer, or by overproduction of XylS alone. Finally, *xylS* and *xylR* are transcribed from the divergent and overlapping promoters *Ps* and *Pr* respectively. The regulation of the latter is connected, because the *Ps* promoter is activated by XylR, which also binds and downregulates its own *Pr* promoter.

Table 3
The mathematical model of the *Ps*/*Pr* promoters of TOL.

Description	Equation
$XylR_i$ concentration	$\frac{dXylR_i}{dt} = \frac{\beta_{XylR_i} Pr_{TC}}{K_{Pr,XylR_i} + Pr_{TC}} - r_{XylR} XylR_i S_1 + 3r_{R,XylR} XylR_a (S_{0,1} - S_1) - \alpha_{XylR_i} XylR_i$
$XylR_a$ concentration	$\frac{dXylR_a}{dt} = \frac{1}{3} r_{XylR} XylR_i S_1 - r_{R,XylR} XylR_a (S_{0,1} - S_1) - \alpha_{XylR_a} XylR_a$
Pr promoter activity	$\frac{dPr_{TC}}{dt} = \frac{\beta_{Pr}}{1+(XylR_i/K_{XylR_i})^{n_{Pr,i}}+(XylR_a/K_{XylR_a})^{n_{Pr,a}}} \frac{1}{1+K_{SUC,Pr}S_2^2} - \alpha_{Pr} Pr_{TC}$
Ps promoter activity	$\frac{dPs_{TC}}{dt} = \beta_0 + \beta_{Ps} \frac{XylR_a^{n_{Ps,a}}}{K_{XylR_a,Ps}^{n_{Ps,a}} + XylR_a^{n_{Ps,a}}} \frac{1}{1+(S_2/K_{SUC,Ps})^2} - \alpha_{Ps} Ps_{TC}$

be supplied additionally to the inhibitory one to support biomass growth. Thus, the growth kinetics of mt-2 was studied in the presence of succinate. Unlike the *m*-xylene only case presented above, the assumption that $S_2 \gg K_{s,2}$ was not valid when only succinate was fed. Therefore, the biodegradation of 13.6 mM succinate fed in a batch experiment was modelled using Eq. (13) for succinate biodegradation and Eq. (14) for biomass growth using the Monod model. Furthermore, the specific succinate consumption rate was independently modelled using Eq. (15) and biomass production was expressed by Eq. (16). Fig. 1D shows that the Monod model can effectively describe the experimental results. The parameter values estimated are listed in Table 2.

$$\frac{dS_2}{dt} = -q_{s,2}X \tag{13}$$

$$\mu_2 = \frac{\mu_{max,2}S_2}{K_{S,2} + S_2} \tag{14}$$

$$q_{s,2} = \frac{R_{max,2}S_2}{K_{s,2} + S_2} \tag{15}$$

$$\frac{dX}{dt} = \mu_2 X \tag{16}$$

3.3. Succinate–*m*-xylene mixture: parameter estimation experiment

The microbial strain was cultured in a batch experiment in the presence of 14 mM succinate and 1.04 mM *m*-xylene. According to the experimental results (Fig. 3), unlike the cases of simultaneous or diauxic growth often met in mixed-substrates, mt-2 presented a different growth pattern. Following the initial lag-phase, *m*-xylene degradation started first followed by succinate degradation resulting in two phases where both substrates were utilised individually and one phase where both substrates were utilised simultaneously.

m-Xylene is sensed by *P. putida* strains bearing the TOL plasmid mainly as a stressor to be extruded rather than as a nutrient to be metabolised. Thus, *m*-xylene causes the reduction of a variety of central carbon metabolism enzymes including the succinic semialdehyde dehydrogenase [33], which catalyses the reaction for the conversion of succinate to succinate semialdehyde. Consequently, the lag-phase in succinate degradation can be attributed to the presence of the stressor and the duration of the lag might depend on the time required to inactivate *m*-xylene. Therefore, although succinate is a more readily degradable compound than *m*-xylene, the biodegradation of the latter preceded the biodegradation of succinate due to the stress response. The biodegradation of the inhibitory substrate prior to the easily degradable one has been previously reported for batch experiments of *Arthrobacter* species fed on glucose and toluene [3]

For the description of biomass growth and depletion of the two substrates during the experiments, several models were used. The model that is usually applied to predict growth on mixtures of substrates, when substrate interactions are not present, is the sum

Table 4
Correlation coefficients between experimental and modelling results.

Experiment	R^2 (biomass)	R^2 (*m*-xylene)	R^2 (succinate)
1	0.994	0.998	–
2	0.990	–	0.996
3 (Combined model)	0.974	0.978	0.987
3 (Competitive inh.)	0.952	0.965	0.953
3 (Non-competitive Inh.)	0.771	0.372	0.860
3 (Un-competitive Inh.)	0.994	0.979	0.969
3 (SKIP model)	0.997	0.974	0.955
4 (Combined model)	0.951	0.977	0.948
4 (Un-competitive inh.)	0.837	0.606	0.956
4 (SKIP model)	0.956	0.844	0.705

1—Single-substrate biodegradation: *m*-xylene only; 2—single-substrate biodegradation: succinate only; 3—succinate–*m*-xylene mixture: parameter estimation experiment; 4—succinate–*m*-xylene mixture: predictive experiment.

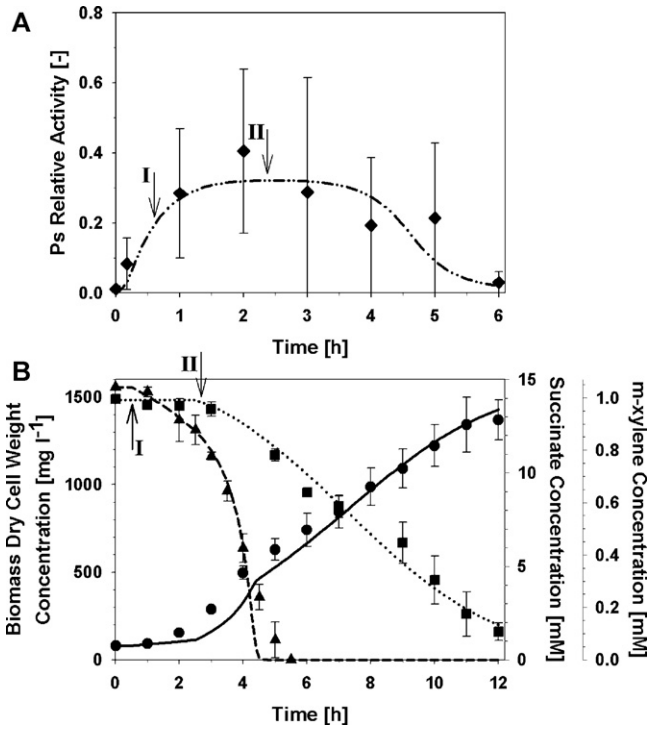

Fig. 3. Prediction of the double-substrate batch biodegradation experiment with the combined genetic circuit–growth kinetic model. (A) *Ps* promoter relative activity, and (B) biomass dry cell weight, *m*-xylene and succinate concentration. I: Beginning of *m*-xylene biodegradation; II: beginning of succinate biodegradation; ♦: *Ps* activity – experimental; ●: biomass dry cell weight concentration – experimental; ■: succinate concentration – experimental; ▲: *m*-xylene concentration – experimental; — · ·: *Ps* activity - predicted; ▬: biomass dry cell weight concentration – predicted; . . . . . .: succinate concentration – predicted; – – -: *m*-xylene concentration – predicted. The *Ps* promoter activity results are obtained as an average from 6 individual measurements for triplicate flasks at each time point and the error bars are calculated for standard deviation.

kinetics model (Eqs. (8), (13) and (17)).

$$\mu = \frac{\mu_{\max,1} S_1}{K_{S,1} + S_1 + (S_1{}^2/K_{I,1}{}^2)} + \frac{\mu_{\max,2} S_2}{K_{S,2} + S_2} \quad (17)$$

This simple model failed to describe the experimental results (data not shown) due to substrate interactions. The presence of *m*-xylene inhibited succinate biodegradation, while the presence of succinate had little effect on *m*-xylene consumption.

Accumulation of metabolic intermediates might be responsible for the inhibitory effects on substrates consumption. The production of methylbenzyl alcohol can be inhibitory for mt-2 [34], while accumulation of 3-methylbenzoate has been also observed in cultures of the strain. Furthermore, *m*-xylene oxidation might result in steric effects on substrate–enzyme interaction [35]. Based on the experimental results presented in Fig. 3 it is apparent that when only succinate is available, from 5.5 h and until the end of the experiment, the cell growth is considerably slower compared to the single-substrate experiment (Fig. 1D). However, inhibition on *m*-xylene consumption was not observed in the mixed-substrate experiment. In order to consider the inhibitory effects of *m*-xylene and its intermediates on succinate degradation a new succinate degradation model is suggested (Eq. (18)) and the specific growth rate on both substrates is given in Eq. (19).

$$\mu_2 = \frac{\mu_{\max,2} S_2}{K_{S,2} + S_2} \frac{K_{I,1,2}}{K_{I,1,2} + S_1} \frac{K_{I,1-P,2}}{K_{I,1-P,2} + (S_0 - S_1)} \quad (18)$$

$$\mu = \frac{\mu_{\max,1} S_1}{K_{S,1} + S_1 + (S_1{}^2/K_{I,1}{}^2)} + \frac{\mu_{\max,2} S_2}{K_{S,2} + S_2} \frac{K_{I,1,2}}{K_{I,1,2} + S_1} \frac{K_{I,1-P,2}}{K_{I,1-P,2} + (S_0 - S_1)} \quad (19)$$

Measurements of the intermediates from *m*-xylene biodegradation would be required to consider their effect on succinate degradation rate. However, since several metabolic intermediates are produced when *m*-xylene is catabolised, the determination of their concentration during the experiments would be a difficult process. For this reason we assume that a major intermediate in *m*-xylene degradation accumulates over time proportionally to the removal of *m*-xylene. Thus, in Eq. (18) the degraded amount of *m*-xylene is used to express the concentration of the inhibitory intermediates, an assumption which is similar to that previously developed for considering the inhibitory effects of metabolic intermediates on phenol degradation by *P. putida* ATCC 49451 [30]. Furthermore, inhibition of growth on succinate due to the presence of *m*-xylene is also considered and the specific succinate consumption rate can be independently modelled using Eq. (20).

$$q_{s,2} = \frac{R_{\max,2} S_2}{K_{s,2} + S_2} \frac{K_{Iq,1,2}}{K_{Iq,1,2} + S_1} \frac{K_{Iq,1-P,2}}{K_{Iq,1-P,2} + (S_0 - S_1)} \quad (20)$$

In the *m*-xylene only experiment, degradation of *m*-xylene starts when the *Ps* promoter's relative activity increases by 65-fold. However, the activity of *Ps* is known to be repressed in the presence of both substrates as compared to when only *m*-xylene is available due to catabolite repression [20]. Therefore due to the overall repression of *Ps*, it was assumed that under the presence of both substrates *m*-xylene degradation started when the activity of *Ps* increased from its basal activity level by 14-fold (Fig. 3A). Furthermore, due to the effect caused by *m*-xylene, reassigning the bulk of the available transcriptional machinery to endure general stress [33], we assume that growth on succinate starts when the cellular metabolic resources are redistributed towards succinate assimilation indicating the onset of the TOL pathway deinduction. This response can be expressed by the time point where *Ps* activity starts decreasing from its maximum value. Based on the combination of the model presented above and the genetic circuit model predicting *Ps* promoter's activity, the experimental results (Fig. 3B) were adequately described. Parameters values $K_{I,1,2}$ and $K_{I,1\text{-}P,2}$ were estimated from the experimental data. The accuracy of the model could be further improved by identifying and measuring the concentration of the inhibitory intermediate from *m*-xylene degradation. This way, the validity of the assumption that the specific intermediate is not degraded over time (Eq. (18)) would be experimentally verified.

3.4. Succinate–m-xylene mixture: prediction with existing models

The substrate interactions observed were modelled with cell growth models accounting for competitive, noncompetitive and uncompetitive inhibition. Substantial differences exist between the experimental data and the prediction of the models (data not shown). In many cases where a mixed-substrate experiment cannot be accurately predicted using enzymatic kinetics, the SKIP model is applied. However, the SKIP model was also unsuccessfully applied to describe the experimental results. Since the above models failed to predict the experimental data, they were applied with the addition of the term accounting for inhibition of cell growth on succinate due to the presence of inhibitory intermediates from *m*-xylene biodegradation. Furthermore, the parameter values of these models were estimated from the single-substrate experiments presented above.

Similarly to succinate, the end products from *m*-xylene biodegradation in the TOL pathway are Krebs cycle intermediates [32]. Therefore, since a part of the metabolic pathway followed in the catabolism of both *m*-xylene and succinate is the same, the two substrates might compete for an enzyme in the pathway. In order to evaluate this scenario, a model incorporating competitive substrate kinetics [36] was applied according to Eq. (21).

$$\mu = \frac{\mu_{\max,1} S_1}{K_{S,1} + S_1 + (K_{S,2}/K_{S,1}) S_2 + (S_1{}^2/K_{I,1}{}^2)} + \frac{\mu_{\max,2} S_2}{K_{S,2} + S_2 + (K_{S,2}/K_{S,1}) S_1} \frac{K_{I,1-P,2}}{K_{I,1-P,2} + (1 - S_1)} \quad (21)$$

The trajectories predicted by this model are shown in Fig. 4A–C using the parameter values determined from the single-substrate experiments and the value of $K_{I,2\text{-}P,1}$ obtained in Section 3.3. This model underpredicted the production of biomass and overpredicted *m*-xylene and succinate concentration profiles for most of the experiment.

A different form of interaction that is commonly used for an enzyme and two substrates is noncompetitive inhibition. In this case, both substrates are simultaneously bound to the enzyme forming a nonreactive complex [37]. Based on this interaction the growth model for noncompetitive inhibition is given in Eq. (22).

$$\mu = \frac{\mu_{\max,1} S_1}{(K_{S,1} + S_1)(1 + (S_2/K_{S,2})) + (S_1{}^2/K_{I,1}{}^2)} + \frac{\mu_{\max,2} S_2}{(K_{S,2} + S_2)(1 + (S_1/K_{S,1}))} \frac{K_{I,1-P,2}}{K_{I,1-P,2} + (1 - S_1)} \quad (22)$$

The model prediction presented in Fig. 4A–C shows that the biomass dry cell weight and the substrates concentration calculated by this model, failed to follow the experimental data as the consumption of both substrates was much faster experimentally than predicted.

A similar type of inhibition to noncompetitive is uncompetitive inhibition. However, in uncompetitive inhibition the inhibitor is able to bind only to the enzyme–substrate complex and not to the free enzyme. The model of cell growth in the presence of uncompetitive inhibition has been previously described [36] according to

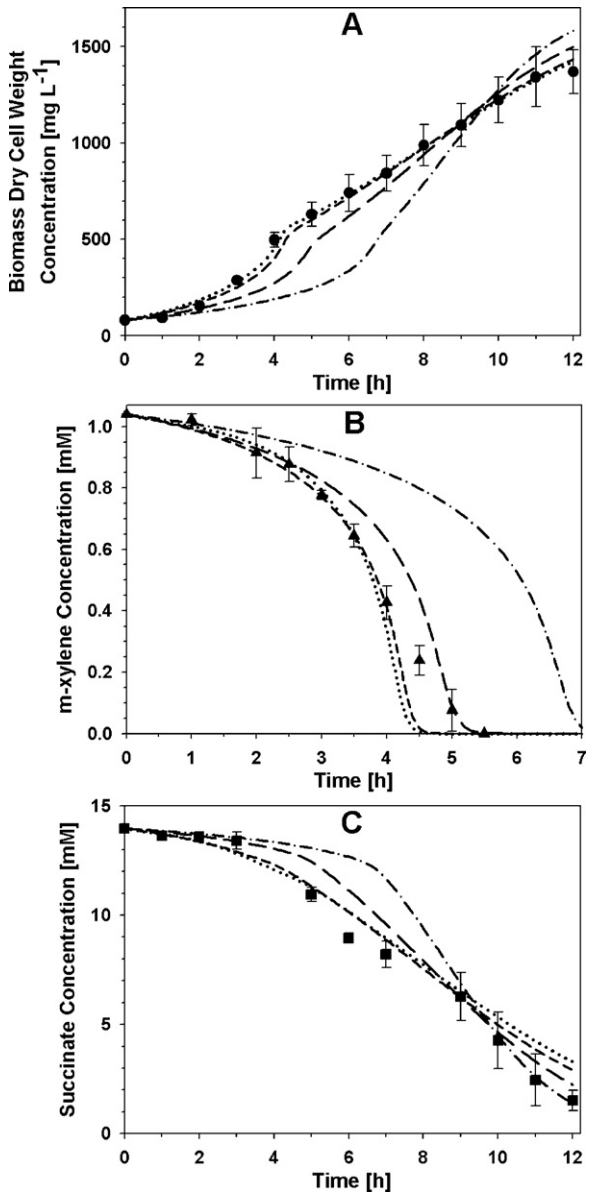

Fig. 4. Comparison of prediction of the double-substrate batch biodegradation experiment from the different substrate interaction models. (A) Biomass dry cell weight concentration, (B) *m*-xylene concentration, and (C) succinate concentration. ●: Biomass dry cell weight concentration – experimental; ■: succinate concentration – experimental; ▲: *m*-xylene concentration – experimental; — —: competitive inhibition model (biomass, *m*-xylene and succinate – predicted); – · – ·: non-competitive inhibition model (biomass, *m*-xylene and succinate – predicted); – – –: uncompetitive inhibition model (biomass, *m*-xylene and succinate - predicted); . . . . . .: unspecified type of inhibition model (biomass, *m*-xylene and succinate – predicted). The error bars are calculated for standard deviation.

Eq. (23).

$$\mu = \frac{\mu_{\max,1} S_1}{K_{S,1} + S_1(1 + (S_2/K_{S,2})) + ({S_1}^3/{K_{I,1}}^2)} + \frac{\mu_{\max,2} S_2}{K_{S,2} + S_2(1 + (S_1/K_{S,1}))} \frac{K_{I,1-P,2}}{K_{I,1-P,2} + (1 - S_1)} \quad (23)$$

Similarly to the combined genetic circuit–growth kinetic model presented above uncompetitive inhibition satisfactorily describes the experimental data (Fig. 4A–C) confirmed by the high correlation coefficient values obtained (Table 4).

Additionally to the three models developed in analogy to enzyme kinetics, the SKIP model that does not specify the type of interaction was also applied. This model includes an interaction parameter $I_{j,k}$ in each Monod term indicating the degree to which substrate *j* affects the biodegradation of substrate *k*. The SKIP model was first formulated by Yoon et al. [36], which is presented in Eq. (24).

$$\mu = \frac{\mu_{\max,1} S_1}{K_{S,1} + S_1 + I_{2,1} S_2 + ({S_1}^3/{K_{I,1}}^2)} + \frac{\mu_{\max,2} S_2}{K_{S,2} + S_2 + I_{1,2} S_1} \frac{K_{I,1-P,2}}{K_{I,1-P,2} + (1 - S_1)} \quad (24)$$

The SKIP model accurately described biomass dry cell weight concentration during the experiment. Furthermore, the prediction of the SKIP model showed minor deviation from the experimentally obtained substrates concentration producing an overall satisfactory prediction of the system. The interaction parameter values were estimated from this experiment and their values are given in Table 2.

3.5. Succinate–m-xylene mixture: predictive experiment

Having confirmed that the combined, competitive inhibition and SKIP models fitted best the parameter estimation experiment, their predictive capability was tested with an independent experiment. The initial succinate concentration was maintained the same as in the parameter estimation experiment (14.1 mM), while *m*-xylene concentration was reduced to 0.8 mM.

The duration of the lag-phase for each substrate was calculated from the genetic circuit model (Fig. 5D). The combined model underpredicted and overpredicted to a minor extent the biomass and succinate concentrations over time respectively, as confirmed by the correlation coefficient values calculated between experimental and modelling results (Table 4). However, the model closely tracked *m*-xylene concentration and overall produced a satisfactory description of the experimental data (Fig. 5A–C). On the contrary, the competitive inhibition and the SKIP model failed to describe the experimental results as confirmed by the values of the correlation coefficient obtained. Interestingly, the SKIP and the enzymatic kinetic models were also unsuccessfully applied to describe both mixed-substrate experiments, using the information from the genetic circuit model to predict the duration of the lag-phase (data not shown). The results presented above confirm that only the combined model can be predictive under different experimental conditions, underlying the importance of incorporating in growth kinetic models information from key genetic circuits.

3.6. Limitations of existing models

The number of modelling studies concentrating in biodegradation of mixed-substrates is limited compared to single-substrate biodegradation. Especially when the substrates are differential, triggering various parts of the cell's metabolism, the modelling process of cellular growth can be very complex resulting in very few modelling studies being published in the particular subject. The most common limitations identified when modelling the biodegradation of mixtures of substrates are summarised in Table 5 and can be divided in three main categories.

In the first category the lag-phase is not modelled and the models developed are used to predict only the post lag-phase period. However, the lag-phase can vary substantially between single-substrate and mixed-substrate biodegradation or when there is a change in the experimental conditions. The lag-phase can be a substantial part of batch processes and therefore the accurate prediction of its duration can be very important for an accurate description of these systems. Furthermore, in continuous appli-

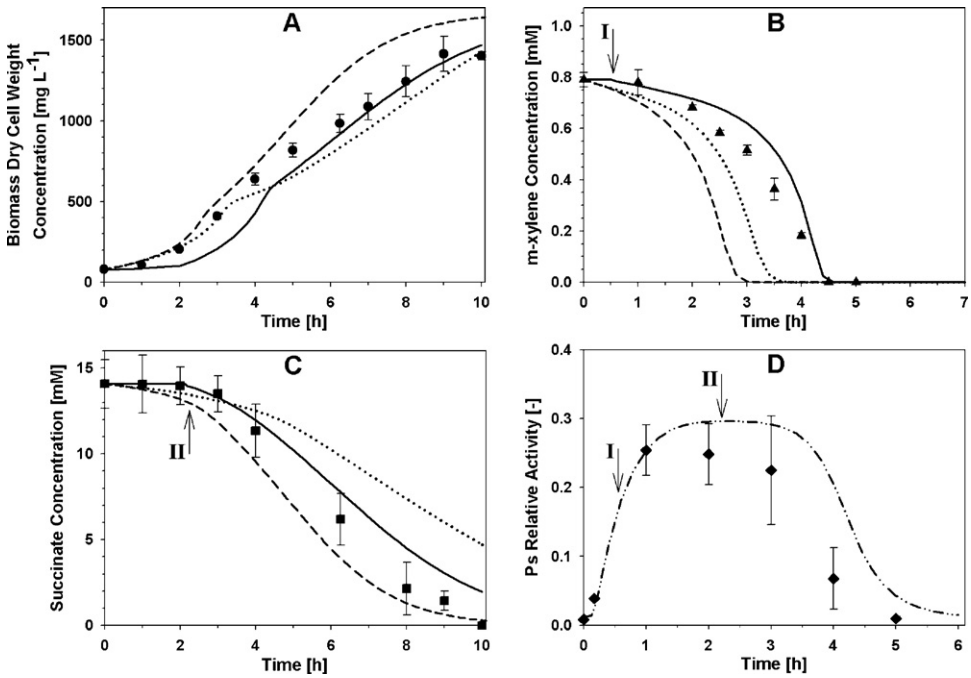

Fig. 5. Comparison of prediction of the model validation batch biodegradation experiment from the different substrate interaction models and the combined genetic circuit–growth kinetic model. (A) Biomass dry cell weight concentration, (B) *m*-xylene concentration, (C) succinate concentration, and (D) *Ps* promoter relative activity. I: Beginning of *m*-xylene biodegradation; II: beginning of succinate biodegradation; ●: biomass dry cell weight concentration - experimental; ■: succinate concentration - experimental; ▲: *m*-xylene concentration – experimental; ♦: *Ps* activity – experimental; ——: combined genetic circuit–growth kinetic model (biomass, *m*-xylene and succinate – prediction); – – –: uncompetitive inhibition model (biomass, *m*-xylene and succinate – prediction); . . . . .: unspecified type of inhibition model (biomass, *m*-xylene and succinate – prediction);— - -: *Ps* activity – predicted. The *Ps* promoter activity results are obtained as an average from 6 individual measurements for triplicate flasks at each time point and the error bars are calculated for standard deviation.

Table 5
Limitations of the existing models.

Substrates	Model type	Limitations
Benzene, toluene, ethylbenzene and o-xylene (BTEX) [10]	SKIP model	Category 1
Benzene, toluene and phenol [6]	SKIP model	Category 1
Phenol, chlorophenol and sodium glutamate (SG) [40]	Empirical kinetic model	Category 3. The utilisation profile of SG is not modelled and SG concentration is correlated using a polynomial function
Phenol and sodium salicylate [43]	Competitive and uncompetitive model	Categories 1 and 3
Naphthalene, phenanthrene and pyrene [8]	Multisubstrate form of the Monod model	Category 2. Biomass simulation results are presented without experimental measurements
Toluene and phenol [4]	SKIP model	Category 2
Phenol and p-cresol [44]	SKIP model	Category 2
Toluene and trichloroethylene (TCE) [45]	Competitive inhibition	Category 3. The kinetic model was not able to predict the TCE removal in the absence of toluene or at very low toluene concentrations
Phenol and toluene [41]	SKIP model	Category 3
Binary and complex mixtures of polycyclic aromatic hydrocarbons (PAHs) [46]	Multisubstrate biodegradation kinetic models: accounting or not accounting for competitive inhibition	Category 3. Neither of the two multisubstrate models was clearly optimal in the present study
Pentachlorophenol and Tween 20 [47]	Contois model with substrate interaction effects	Category 3. Finding a single set of kinetic parameters that predicted all dual substrate tests was not achieved
Benzene, toluene, and p-xylene [48]	Competitive inhibition	Category 2
Glucose and 2,4-dichlorophenoxyacetate [49]	Monod model accounting for inhibition by alternative substrates	Category 2
Glucose and aniline [50]	SKIP model	Category 2
Phenol and 4-chlorophenol [51]	Empirical kinetic model	The duration of the lag period is based on a fitted curve of the initial substrate concentration vs the lag period duration, for only a narrow substrate concentration range

The most common limitations identified have been grouped in three main categories. Category 1: the lag period is not modelled and the models are used to predict only the post lag-phase data; Category 2: there is no comparison of the model's prediction against an independent experiment; Category 3: the model predictions do not fit accurately the experimental results and it is not possible to predict a variety of multisubstrate experiments using a single set of parameters.

cations with unstable substrates feed (e.g. fluctuating substrates concentration, starvation periods, sequentially alternating substrates), which is commonplace at remediation sites [38], the duration of the lag can be even harder to predict due to excessive biomass inhibition or inactivation and biomass might require longer time periods to re-establish its full biodegradation capacity [39]. The failure of models to predict the lag-phase in some cases highlights the importance of including in our models the exact mechanism for the production of enzymes with the incorporation of the function of specific genetic circuits producing these enzymes.

Another common limitation, which has been reported for several modelling studies on biodegradation of mixed-substrates, is when the predictive capability of the model is questionable. In most of these cases there is no comparison of the model's prediction against an independent experiment and the predictive capability of the model has only been tested with experimental data which have been also used for estimation of the model parameters.

Various modelling studies cannot accurately predict the experimental results. It is evident that in many cases the models developed are not optimal and it is not possible to predict a variety of multisubstrate experiments using a single set of parameters. Likewise, in some cases the modelling process for the biodegradation of mixed-substrates is very complex and it is simplified with the exclusion of the utilisation profile of a substrate or biomass concentration, which is often correlated using a polynomial function [40]. Furthermore, in cases where a mixture of substrates is degraded by a mixture of microorganisms, interactions between the microorganisms might also occur in conjunction with the substrates interactions making the modelling process even more complex [41]. Therefore, although the determination of which model fits best to the experimental data might indicate the nature of substrates interactions, none of these models might accurately fit the experimental data and the interaction indicated might not be valid over a wide range of conditions [10]. Potential reasons for deviation from enzymatic inhibition can be interactions at the level of substrate transport into the cytoplasm, interactions with regulatory compounds or the presence of catabolic pathways which have not been identified yet [6]. Therefore, the substrate interactions that often occur cannot be accurately described using enzymatic kinetics and their true mechanisms should be considered in a mathematical model describing the function of key genetic circuits controlling the production of enzymes. Also, since bioremediation is often achieved by mixtures of microorganisms, in such cases the modeller should even consider the molecular cell–cell communication mechanisms altering the function of key genetic circuits [42]. In line with the above, the combined model constitutes an improvement of the currently used models for predicting microbial growth kinetics and it has been used to predict the concentration of biomass and of both differential substrates under a variety of conditions.

4. Conclusions

There is a need for the development of modelling approaches that account for gene regulation to describe unusual substrate interactions. The mathematical model presented in this study successfully combines the prediction of a key genetic circuit for the bioprocess to the growth kinetics of the microorganism, producing a reliable description of the system's performance. Although the genetic circuit model was simulated from the beginning of the experiments to predict the duration of the lag-phase, the growth kinetic model could only be applied after the lag. The results show that it is possible to couple genetic information to metabolic models improving the prediction of bioprocesses with increased modelling complexity that currently used models fail to predict. Thus, with the use of advanced genetic and biochemical techniques additional information about complex bioprocesses could be obtained facilitating the development of combined models accurately predicting their behaviour. Following this approach, we could eventually have activity levels of key genes, controlling upstream the production of catabolic enzymes, linked to the cellular kinetics. Furthermore, apart from the development of models used for the design, control and optimisation of bioprocesses, the methodology of combining key molecular interactions to growth kinetics can offer the prospect of making model-driven questions on biology. In this way, certain biological hypothesis can be either validated or disproved, assisting to further our understanding of cellular mechanisms.

Acknowledgements

This work was supported by the European Union with the following projects: (a) PROBACTYS (FP6 – NEST-PATHFINDER EU call on Synthetic Biology), (b) PSYSMO (BBSRC – ERA-NET program on the Systems Biology of Microorganisms) and (c) TARPOL (FP7 EU – KBBE Coordination Action for SynBio in Environmental Sciences). We would like to thank Dr. Ioannis Vyrides for his valuable help with the HPLC analysis.

Appendix A. Supplementary data

Supplementary data associated with this article can be found, in the online version, at doi:10.1016/j.bej.2011.03.012.

References

[1] K. Kovarova-Kovar, T. Egli, Growth kinetics of suspended microbial cells: from single-substrate-controlled growth to mixed-substrate kinetics, Microbiol. Mol. Biol. Rev. 62 (1998) 646–666.
[2] B.C. Baltzis, A.G. Fredrickson, Limitation of growth rate by two complementary nutrients: some elementary but neglected considerations, Biotechnol. Bioeng. 31 (1987) 75–86.
[3] S. Kar, T. Swaminathan, A. Baradarajan, Studies on biodegradation of a mixture of toxic and nontoxic pollutant using *Arthrobacter* species, Bioprocess. Eng. 15 (1996) 195–199.
[4] J.B. Rogers, K.F. Reardon, Modeling substrate interactions during the biodegradation of mixtures of toluene and phenol by *Burkholderia* species JS150, Biotechnol. Bioeng. 70 (2000) 428–435.
[5] W. Harder, L. Dijkhuizen, Strategies of mixed substrate utilisation in microorganisms, Philos. Trans. R. Soc. Lond. B 297 (1982) 459–480.
[6] K.F. Reardon, D.C. Mosteller, J.D.B. Rogers, Biodegradation kinetics of benzene, toluene, and phenol as single and mixed substrates for *Pseudomonas putida* F1, Biotechnol. Bioeng. 69 (2000) 385–400.
[7] D. Millette, J.F. Barker, Y. Comeau, B.J. Butler, E.O. Frind, B. Clement, R. Samson, Substrate interaction during aerobic biodegradation of creosote-related compounds: a factorial batch approach, Environ. Sci. Technol. 29 (1995) 1944–1952.
[8] S. Guha, C.A. Peters, P.R. Jaffe, Multisubstrate biodegradation kinetics of naphthalene, phenanthrene, and pyrene mixtures, Biotechnol. Bioeng. 65 (1999) 491–499.
[9] J. Monod, The growth of bacterial cultures, Annu. Rev. Microbiol. 3 (1949) 371–394.
[10] J.V. Littlejohns, A.J. Daugulis, Kinetics and interactions of BTEX compounds during degradation by a bacterial consortium, Process. Biochem. 43 (2008) 1068–1076.
[11] N.B. Pamment, R.J. Hall, J.P. Barford, Mathematical modeling of lag phases in microbial growth, Biotechnol. Bioeng. 20 (1978) 349–381.
[12] R. Weiss, Challenges and opportunities in programming living cells, The Bridge 33 (2003) 39–46.
[13] M.T. Laub, L. Shapiro, H.H. McAdams, Systems biology of *Caulobacter*, Annu. Rev. Genet. 41 (2007) 429–441.
[14] F.J. Isaacs, J. Hasty, C.R. Cantor, J.J. Collins, Prediction and measurement of an autoregulatory genetic module, Proc. Natl. Acad. Sci. U.S.A. 100 (2003) 7714–7719.
[15] M.B. Elowitz, S. Leibler, A synthetic oscillatory network of transcriptional regulators, Nature 403 (2000) 335–338.
[16] P.E. Hardin, The circadian timekeeping system of *Drosophila*, Curr. Biol. 15 (2005) R714–R722.
[17] J. Kim, K.S. White, E. Winfree, Construction of an in vitro bistable circuit from synthetic transcriptional switches, Mol. Syst. Biol. 2 (2006) 68.
[18] D. Sprinzak, M.B. Elowitz, Reconstruction of genetic circuits, Nature 438 (2005) 443–448.
[19] K. Bettenbrock, S. Fischer, A. Kremling, K. Jahreis, T. Sauter, E.-D. Gilles, A quantitative approach to catabolite repression in *Escherichia coli*, J. Biol. Chem. 281 (2006) 2578–2584.

[20] M. Koutinas, M.-C. Lam, A. Kiparissides, R. Silva-Rocha, M. Godinho, A.G. Livingston, E.N. Pistikopoulos, V. de Lorenzo, V.A.P. Martins dos Santos, A. Mantalaris, The regulatory logic of *m*-xylene biodegradation by *Pseudomonas putida* mt-2 exposed by dynamic modelling of the principal node *Ps*/*Pr* of the TOL plasmid, Environ. Microbiol. 12 (2010) 1705–1718.
[21] J. Sambrook, E.F. Fritsch, E. Maniatis, Molecular Cloning: A Laboratory Manual, Cold Spring Harbour Press, New York, 1989.
[22] Process Systems Enterprise, *gPROMS*. www.psenterprise.com/gproms, 1997–2010.
[23] J. Morgado, G. Merlin, Y. Gonthier, A. Eyraud, A mechanistic model for *m*-xylene treatment with a peat-bed biofilter, Environ. Technol. 25 (2004) 123–132.
[24] J.F. Andrews, A mathematical model for the continuous culture of microorganisms utilizing inhibitory substrates, Biotechnol. Bioeng. 10 (1968) 707–723.
[25] S. Aiba, M. Shoda, M. Nagatani, Kinetics of product inhibition in alcohol kinetics, Biotechnol. Bioeng. 10 (1968) 845–864.
[26] T. Yano, S. Koga, Dynamic behaviour of chemostat subject to substrate inhibition, Biotechnol. Bioeng. 11 (1969) 139–153.
[27] M. Wayman, M.C. Tseng, Inhibition threshold substrate concentrations, Biotechnol. Bioeng. 18 (1976) 383–387.
[28] J.H.T. Luong, Generalization of Monod kinetics for analysis of growth data with substrate inhibition, Biotechnol. Bioeng. 29 (1987) 242–248.
[29] G. Alagappan, R.M. Cowan, Biokinetic models for representing the complete inhibition of microbial activity at high substrate concentrations, Biotechnol. Bioeng. 75 (2001) 393–405.
[30] S.-J. Wang, K.-C. Loh, Modeling the role of metabolic intermediates in kinetics of phenol biodegradation, Enzyme Microb. Technol. 25 (1999) 177–184.
[31] K.N. Timmis, *Pseudomonas putida*: a cosmopolitan opportunist *par* excellence, Environ. Microbiol. 4 (2002) 779–781.
[32] J.L. Ramos, S. Marques, K.N. Timmis, Transcriptional control of the *Pseudomonas* TOL plasmid catabolic operons is achieved through an interplay of host factors and plasmid-encoded regulators, Annu. Rev. Microbiol. 51 (1997) 341–372.
[33] P. Dominguez-Cuevas, J.-E. Gonzalez-Pastor, S. Marques, J.-L. Ramos, V. de Lorenzo, Transcriptional tradeoff between metabolic and stress-response programs in *Pseudomonas putida* KT2440 cells exposed to toluene, J. Biol. Chem. 281 (2006) 11981–11991.
[34] W.A. Duetz, B. Wind, J.G. van Andel, M.R. Barnes, P.A. Williams, M. Rutgers, Biodegradation kinetics of toluene, *m*-xylene, *p*-xylene and their intermediates through the upper TOL pathway in *Pseudomonas putida* (pWW0), Microbiology 144 (1998) 1669–1675.
[35] R.H Olsen, J.J. Kukor, B. Kaphammer, A novel toluene-3-monooxygenase pathway cloned from *Pseudomonas pickettii* PKO1, J. Bacteriol. 176 (1994) 3749–3756.
[36] H. Yoon, G. Klinzing, H.W. Blanch, Competition for mixed substrates by microbial populations, Biotechnol. Bioeng. 19 (1977) 1193–1210.
[37] I.H. Segel, Enzyme Kinetics, John Wiley & Sons, New York, 1975.
[38] M. Koutinas, I.I.R. Baptista, A. Meniconi, L.G. Peeva, A. Mantalaris, P.M.L. Castro, A.G. Livingston, The use of an oil-absorber-bioscrubber system during biodegradation of sequentially alternating loadings of 1,2-dichloroethane and flurobenzene in a waste gas, Chem. Eng. Sci. 62 (2007) 5989–6001.
[39] J. Park, J. Lang, K. Thamaraiselvi, J.J. Kukor, L.M. Abriola, Induction kinetics of aerobic toluene degradation as a function of carbon starvation history, Process. Biochem. 43 (2008) 1345–1351.
[40] S.-J. Wang, K.-C. Loh, Biotransformation kinetics of *Pseudomonas putida* for cometabolism of phenol and 4-chlorophenol in the presence of sodium glutamate, Biodegradation 12 (2001) 189–199.
[41] J.B. Rogers, N.M. DuTeau, K.F. Reardon, Use of 16S-rRNA to investigate microbial population dynamics during biodegradation of toluene and phenol by a binary culture, Biotechnol. Bioeng. 70 (2000) 436–445.
[42] L.C. You, R.S. Cox, R. Weiss, F.H. Arnold, Programmed population control by cell–cell communication and regulated killing, Nature 428 (2004) 868–871.
[43] R.-S. Juang, S.-Y. Tsai, Growth kinetics of *Pseudomonas putida* in the biodegradation of single and mixed phenol and sodium salicylate, Biochem. Eng. J. 31 (2006) 133–140.
[44] Z. Alexieva, M. Gerginova, J. Manasiev, P. Zlateva, N. Shivarova, A. Krastanov, Phenol and cresol mixture degradation by the yeast *Trichosporon cutaneum*, J. Ind. Microbiol. Biotechnol. 35 (2008) 1297–1301.
[45] J.P. Arcangeli, E. Arvin, Modeling of the cometabolic biodegradation of trichloroethylene by toluene oxidizing bacteria in a biofilm system, Environ. Sci. Technol. 31 (1997) 3044–3052.
[46] C.D. Knightes, C.A. Peters, Multisubstrate biodegradation kinetics for binary and complex mixtures of polycyclic aromatic hydrocarbons, Environ. Toxicol. Chem. 25 (2006) 1746–1756.
[47] A.R. Bielefeldt, T. Cort, Dual substrate biodegradation of a nonionic surfactant and pentachlorophenol by *Sphingomonas chlorophenolica* RA2, Biotechnol. Bioeng. 89 (2005) 680–689.
[48] H. Yu, B.J. Kim, B.E. Rittmann, A two-step model for the kinetics of BTX degradation and intermediate formation by *Pseudomonas putida* F1, Biodegradation 12 (2001) 465–475.
[49] A.C. Papanastasiou, W.J. Maier, Kinetics of biodegradation of 2,4-dichlorophenoxy-acetate in the presence of glucose, Biotechnol. Bioeng. 24 (1982) 2001–2011.
[50] U.S. Zissi, G.C. Lyberatos, Kinetics of growth and aniline degradation by *Stenotrophomonas maltophilia*, Water Environ. Res. 71 (1999) 43–49.
[51] G.A. Hill, B.J. Milne, P.A. Nawrocki, Cometabolic degradation of 4-chlorophenol by *Alcaligenes eutrophus*, Appl. Microbiol. Biotechnol. 46 (1996) 163–168.